



GEOSCIENCES

Short-term glacier area changes, glacier geometry dependence, and regional climatic variations forcing, King George Island, Antarctica

JÚLIA L. LORENZ, KÁTIA K. DA ROSA, CARINA PETSCH, CLEIVA PERONDI,
FILIPE D. IDALINO, JEFFREY DANIEL AUGER, ROSEMARY VIEIRA &
JEFFERSON C. SIMÕES

Abstract: This study investigates the transient snowline (TSL) altitude for summer 2020, as well as glacial area loss in King George Island Icefields since 1988 using Sentinel-1 and 2 and Landsat Thematic Mapper (TM) imagery. Trends and anomalies in atmospheric temperature, U-wind, and V-wind were examined using ERA5 solutions. Results show the wet-snow zone corresponds to values of $\leq -13\text{dB}$, and 44.3% of the glacial area is located above the TSL ($\geq 300\text{ m}$). Glacial area for 2020 is 999.95 km^2 , and losses in the period represent 104.9 km^2 (error $<1\%$) – a retreat of $3.17\text{ km}^2 / \text{year}$. Glaciers in Keller Peninsula and Bellingshausen Dome lost the most area (28% and 17%, respectively) and did not have a TSL in 2020; followed by Warszawa (15%), Kraków (13%), and Eastern (10%), where the TSL was verified. Percentage area loss values increased with decreases in dimensions, area above TSL, and maximum elevation. Calving glaciers with ice-flow toward deeper and steeper submarine sectors (Bransfield Strait) exhibited greater glacier variations. The trend in warming atmospheric temperature was greater in the Bransfield Strait than in the Drake Passage. TSL and retreat difference between glaciers were influenced by climatic and ocean input, as well as multiple environmental factors.

Key words: climate change, glacier fluctuations, NDSI, Sentinel, snowline.

INTRODUCTION

Over the last few decades, glaciers have been retreating and losing volume on a global scale because of anthropogenic atmospheric warming (Roe et al. 2017, Li et al. 2019, Hock & Huss 2021). Hugonnet et al. (2021) reported that glaciers worldwide lost a total mass of 267 ± 16 gigatons per year between 2000 and 2019. According to the sixth IPCC report (2021), climate change has intensified at a rate greater than that observed during the last 6500 years of the Holocene. Human influence is likely the primary cause of glacier retreat at the poles and other latitudes since the 1990s.

Several studies have shown that the Antarctic Peninsula (AP) and the Antarctic subpolar region have experienced increased rapid regional warming during recent decades (King & Harangozo 1998, Kejna 1999, Vaughan et al. 2003, Ferron et al. 2004, Meredith & King 2005, Aquino et al. 2006, Kejna et al. 2013, Simões et al. 2015). The total number of days with positive air temperature has increased for the AP in period 1979-2019 (Turner et al. 2021). These changes could be associated with an increase in greenhouse gas emissions and other factors, such as stratospheric ozone loss and the extent of sea ice cover (Turner et al. 2021).

Following decades of increasing atmospheric air temperatures, some authors (Carrasco 2013, Turner et al. 2016, Oliva et al. 2017, Bozkurt et al. 2020) recorded a cooling period that began in the 1990s. According to Oliva et al. (2017), this recent cooling during 1997/1998 was seasonally variable and more pronounced during the fall and winter in the N-NE portion of the AP and the South Shetlands Islands (SSI). More recent data suggest that this hiatus in atmospheric air temperature increase may have ended in 2010 (Carrasco et al. 2021).

Glacier responses to climate change may vary depending on the period and location of the study area (Pudełko et al. 2018, Li et al. 2019, Silva et al. 2020). Thus, it is essential to establish continuous monitoring of glaciers, which is typically accomplished by remote sensing (Morris et al. 2006, Silverio & Jaquet 2012, Sanches et al. 2015, Rekowsky et al. 2019) because of their large size and remoteness (Gjermundsen et al. 2011, Pan et al. 2012, Paul et al. 2015). Several studies in Antarctica have successfully used optical imaging to monitor glaciers (Simões et al. 2015, Sotille et al. 2016, Pudełko et al. 2018, Hillebrand et al. 2019, Oliveira et al. 2019, Silva et al. 2020).

In general, monitoring results for the AP and Maritime Antarctica glaciers show that they are receding, primarily as a consequence of increasing mean atmospheric temperatures. Additionally, studies have linked tidewater glacier retreat to sea-level rise (Cook et al. 2005, 2016, Davies et al. 2012).

The subpolar maritime region of Antarctica, where King George Island (KGI) is located, is a crucial monitoring area for understanding glacier responses to changes in air temperature (Simões et al. 1999). According to one of the most recent orbital remote sensing data mapping across the KGI glacial area (Braun & Rau 2000), glaciers covered 93% of the island in 1996/1997 (1.250 km²), justifying the need to

update the data. In addition, glaciers located in the peripheral portion of Antarctica could significantly contribute to potential future sea level rise (Edwards et al. 2021, Hugonnet et al. 2021).

This study utilizes orbital remote sensing data to investigate the area and the transient snowline altitude (TSL altitude) of icefields and glaciers in KGI for the year 2020 and compares it to the data for the same from the years 1988/89. Furthermore, this research contributes to the understanding and continuous monitoring of the effects of climate change in the cryosphere using remote sensors. Finally, this study provides data for use in other KGI research projects, such as the monitoring of ice-free zones.

MATERIALS AND METHODS

Study area and background

KGI is the largest of the SSI (Simões et al. 1999, Blindow et al. 2010, Osmanoglu et al. 2013), and it is located north of the AP, between 57°35' and 59°02'W, and 61°54' and 62°16' S (Simões et al. 1999, Blindow et al. 2010). According to Osmanoglu et al. (2013), KGI is approximately 70 km long and 25 km wide, with topography elevated up to 700 m. The icefields on the island include: Arctowski Icefield (AI), Warszawa Icefield (WI), Krakow Icefield (KI), central part (CP), eastern part (EP); the Bellingshausen Dome (BD) was also considered, along with some glaciers present on the Keller Peninsula (KP) (Figure 1). According to Rückamp et al. (2012), ice velocities range from 0.7 m a⁻¹ at domes and dividers to 112.1 m a⁻¹ along steep slopes and outlet glaciers. Between 2008 and 2011, Osmanoglu et al. (2013) highlighted maximum ice surface speeds reached >225 m a⁻¹. The total ice discharge for the analyzed flux gates of KGI was estimated to be 0.720 ± 0.428 Gt a⁻¹.

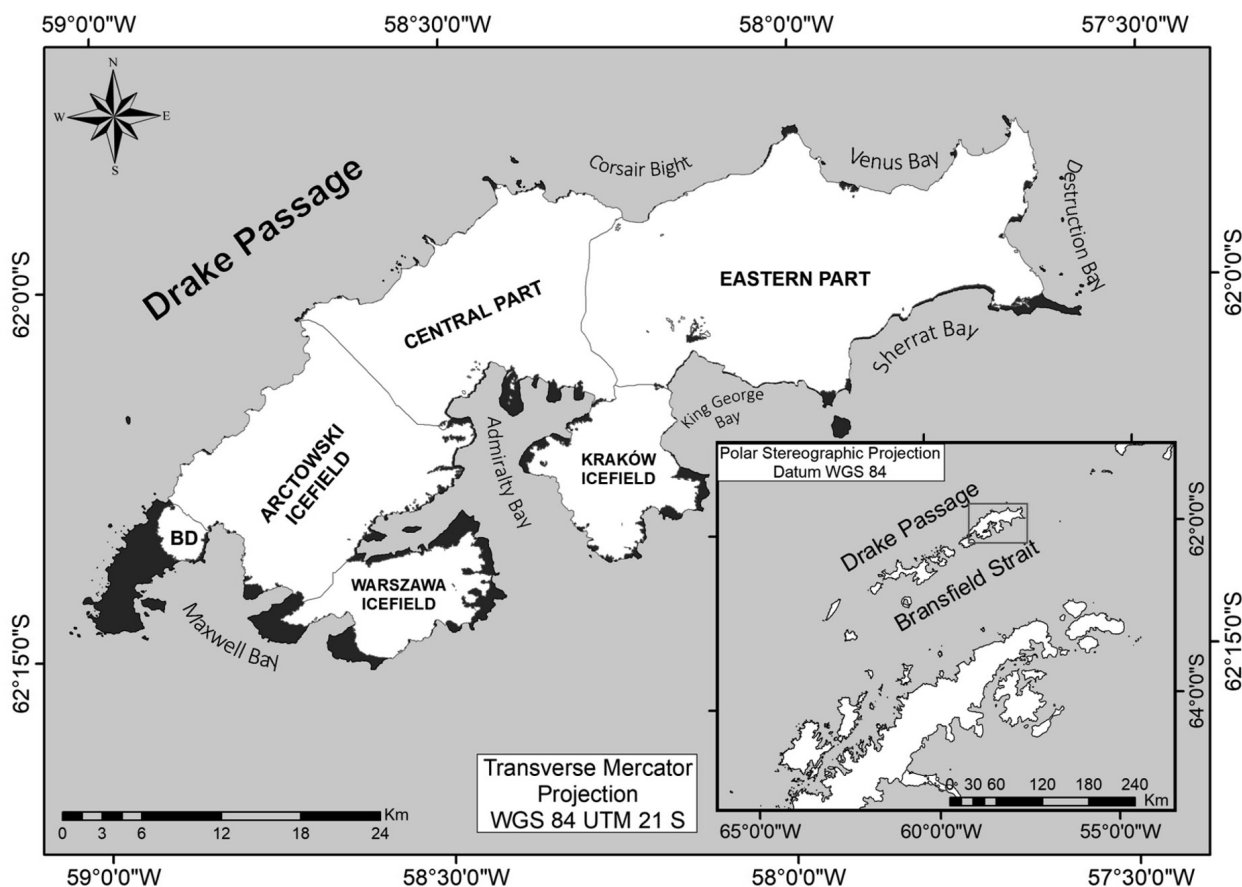


Figure 1. Location of KGI, including its ice fields, South Shetlands, Drake Passage (DP), Bransfield Strait (BS) and its bays. BD: Bellingshausen Dome.

Precipitation in KGI is characterized by high annual variability, with an estimated average of 701.3 mm during the 1968–2011 period (Kejna et al. 2013). The observed annual average air temperature was approximately -1.5°C , with the average warmest month being January (2.4°C) and the coldest was June (-5.6°C) (2012 observations) (Sobota et al. 2015).

Glacier monitoring in KGI highlights their retreat in different periods and geographical portions. These include: (i) The Admiralty Bay between 1979 and 2000 (Arigony-Neto et al. 2001); (ii) The KI glaciers between 1988 and 2017 (Oliveira et al. 2019), as well as the transformation of marine glaciers to non-marine glaciers and new ice-marginal lakes (Perondi et

al. 2020, Petsch et al. 2020; Oliveira et al. 2021); (iii) The BD between 1980 and 2000 (Braun & Goßmann 2002, Rückamp et al. 2011, Simões et al. 2015); (iv) The Polar Club glacier between 1986 and 2011 (Poelking et al. 2014); (v) The Wanda Glacier and Ecology during the period 1979–2010 (Rosa et al. 2009, 2015a); (iv) The Dragon glacier between 1979 and 2010 (Rosa et al. 2014), and for glaciers facing the eastern sector of the WI between 1961 and 1996 (Kejna et al. 1998), 1979 and 2017 (Pudętko et al. 2018, Sziłto & Białik 2018, Perondi et al. 2019, 2020), and between 1979 and 2020 (Rosa et al. 2020); Finally, (iv) the Sphinx and Ecology Glacier between 1979 and 2012 (Sobota et al. 2015). There is also an increase in the number of lakes in some southern sectors

of the island that face bays (Rosa et al. 2020, Oliveira et al. 2021).

Given that the other important pattern is the behavior of the TSL to understand the pattern of the glacier, and this will be the level at which snow turns to solid ice (also referred to as the firn line) and is used to estimate the ELA (Bakke & Nesje 2011, Falk et al. 2018). The final height of the TSL at the end of the melting season is subject to climatic variability and thus varies from year to year (Konz, 2011). According to Falk et al. (2018) the transient snowline altitude in KGI was determined to be near 250 m.s.l. at the end of February 1997 (late-summer snowline) and it was regarded as an approximation of the ELA for the 1996/97 ablation season. It is possible to detect the TSL altitude through remote sensing images and a Digital Elevation Model (DEM). This study utilized radar images because the radar signal can penetrate the ice or snow surface of the glacier zones (Rau et al., 2000).

Database

The Sentinel-2B image was acquired in the middle of the ablation season due to cloud cover in some sectors on dates near the end of the ablation season. The Sentinel-1 IW image was selected because it is photogrammetrically similar to the image used in the most recent KGI study carried out by Braun et al. (2000). This allows for distinguishing the zones.

Glacial drainage dividers provided by the Global Land Ice Measurements from Space (GLIMS) were used to map the area during the 1980s and the 2020s. Data from the Quantartica project, such as bathymetric data, and the Antarctic Digital Database (ADD), such as the coastline, were also used (Gerrish et al. 2020).

ERA5 data were used in this study to analyze trends and anomalies in atmospheric temperature and wind (U-Wind, V-Wind). ERA5 solutions were placed on a 0.5-degree resolution grid. Precipitation and temperature data for

Table I. Database used in the study.

Data/Sensor	Date	Bands	Spatial Resolution	Data type	Source
Landsat 4 TM	02/27/1988	1, 2, 3, 4 e 5	30 m	Optical	https://earthexplorer.usgs.gov/
Landsat 4 TM	01/28/1989	3,2,1	30 m	Optical	https://earthexplorer.usgs.gov/
Sentinel-2B	01/19/2020	2, 3, 4, 8 / 11	10 m and 20 m	Optical	https://scihub.copernicus.eu/dhus/#/home
Sentinel-1 IW HH	03/20/2020	C	5x20 m	SAR	https://scihub.copernicus.eu/dhus/#/home
TanDEM-X	2016	X	12 m	Digital Elevation Model (DEM)	https://doi.pangaea.de/10.1594/PANGAEA.863567
IBCSO	2013	-	500 m x 500 m	Digital Batymetric Model (DBM)	https://doi.pangaea.de/10.1594/PANGAEA.805736
GLIMS	2000	-	-	-	https://www.glims.org/
<i>Antarctic Digital Database (ADD)</i>	-	-	-	-	https://www.scar.org/resources/antarctic-digital-database/
Quantartica	-	-	-	-	https://www.npolar.no/quantartica/
ERA5	-	-	-	-	https://www.ecmwf.int/en/forecasts/datasets/reanalysis-datasets/era5

four days prior to the Sentinel 1 IW image were obtained from the Chilean Meteorological Service (Dirección Meteorológica de Chile), since the Brazilian Comandante Ferraz Antarctic Station (-62.08°S, -58.39°W; 5 m a.s.l.), installed by the Brazilian National Institute for Space Research (INPE), provided data for the 1986–2013 period (Monitoring was only activated in 2022).

Image pre-processing

Sentinel-1 IW Level-1 Ground images were pre-processed using the Sentinel Application Platform (SNAP) and European Space Agency tutorial (2021) as well Zhou et al. (2021) have applied to, excluding the mosaicking of the images. A subset of the study area was created, and the Orbit File was used to incorporate information about the satellite's position and speed. Subsequently, we applied thermal noise removal and performed calibration to adjust the backscatter values. To correct image distortions, range-Doppler terrain correction was used with the DEM GETASSE30 provided by the software for image orthorectification, the DEM by Braun et al. (2016) can be applied in future works to evaluate the results of the range-Doppler terrain because with REMA (Howat et al. 2019) showed problems of spatial coverage for some coastal portions and that could not be neglected, since they constitute areas of interest for this research. Velho et al. (2011) suggested using the Lee filter. The Lee sigma filter of the Speckle-Filter tool was applied with a 3 × 3 window in the calibrated images (Da Rosa et al. 2020). The Lee filter with a 5 × 5 window was applied to reduce speckle noise. Other windows were tested, but the 5 × 5 showed a decrease in noise. Landsat 4 TM images were co-registered with the 2020 Sentinel-2B image, with less than 1-pixel error. In image registration, an error of ± 1 pixel was observed by other authors (Nie et al. 2013, Li et al. 2020). The semi-automatic classification

(SCP) (Congedo 2016) complement was used in the QGIS 3.10.2 software, with the Dark-Object Subtraction (DOS) method for atmospheric correction of optical images.

NDSI and NDWI and mapping validation

To monitor the study region, shapefiles with the new area values for KGI were generated using image interpretation techniques, manual vectorization, and semi-automatic mapping using the normalized difference snow index (NDSI) (Dozier 1989, Hall et al. 1995a) and the normalized difference water index (NDWI) (Mcfeeters 1996). Validation was based on eight control points collected with a Garmin GPS during the OPERANTAR XXXVIII expedition in February 2020 and used to differentiate targets.

As demonstrated by other authors, the Landsat 4 TM (Dozier 1984) and Sentinel-2B (Hillebrand et al. 2019) can distinguish between snow, ice, and clouds. NDSI was specifically chosen because it is an index that facilitates the differentiation of these targets and has been used successfully by other authors (Albert 2002, Morris et al. 2006, Silverio & Jaquet 2012, Sanches et al. 2015, Rekowsky et al. 2019, Hillebrand et al. 2019). This index is calculated using the green and SWIR bands, which distinguish these targets because snow and ice reflect more in the visible (Racoviteanu et al. 2008); however, for the 1.57–1.78 μm range, snow has low reflectance and targets such as clouds have high reflectance (Dozier 1984, Hall et al. 1995b). The following band ratio was used to generate the NDSI for each sensor:

$$NDSI (S2) = \frac{(Band\ 3) - (Band\ 11)}{(Band\ 3) + (Band\ 11)}$$

$$NDSI (L4) = \frac{(Band\ 2) - (Band\ 5)}{(Band\ 2) + (Band\ 5)}$$

NDWI has also been successfully used in Antarctica to monitor aqueous environments

(Oliveira et al. 2021, Rosa et al. 2021). It is calculated from the following band ratio:

$$NDWI (S2) = \frac{(Band\ 3) - (Band\ 8)}{(Band\ 3) + (Band\ 8)}$$

$$NDWI (L4) = \frac{(Band\ 2) - (Band\ 4)}{(Band\ 2) + (Band\ 4)}$$

Following the union of NDSI and NDWI, rasters were transformed into shapefiles (Figure 2) based on the generated classes (rock, cloud, glacier, and water). Consequently, targets that did not correspond to the framed class, such as rock-faced pixels covered in fresh snow, could be excluded from the analysis. Pixels with no values were excluded from the analysis. The generated vector file was intersected with the GLIMS vectors to divide the area by glacial drainage dividers. Because of the presence of clouds in the region, some cloud pixels were superimposed on the glaciers and were considered in the quantification of the glacier area, as were some water pixels due to the presence of supraglacial water over glaciers. The mapping errors and uncertainties were quantified according to Stokes et al. (2019).

Generation of transient snowline altitude and radar zones

Because cloud cover can limit the availability of optical images (Favras et al. 2020), the use of active sensors in monitoring the study area is beneficial. Following the methodology proposed by Zhou & Zheng (2017), two radar zones were identified in the Sentinel-1 IW image using backscatter and altitude (2020).

A zone between -15 dB and -17 dB was identified and considered to be a bare ice zone through visual interpretation of the image. Lower values were discovered at lower elevations (< 300 m), primarily near the Drake Passage (DP) coast. The TSL minimum altitude for KGI on March 20, 2020, was 300 m elevation. This was determined by interpretation of the SAR image.

A new raster for the area was created based on these limits, which were then transformed into a shapefile and intersected with the GLIMS glacial drainage limits. Some targets, such as rock outcrops or shadow areas, were manually deleted.

Statistical analysis

Graphs of mean and standard error were generated for the glaciers facing the DP sector and those facing the Bransfield Strait (BS) sector to better understand the results and dynamics at work in KGI. The EP was used as a case study to compare data regarding percent area loss, percent area above TSL altitude, and bathymetry. Statistical analyses of the EP were also performed. This area had significant percentage losses compared to the icefields with the highest elevation. This area also had glaciers facing both sectors of the KGI, with those facing the BS in more open bays.

RESULTS

Radar zones e TSL altitude

Prior to the acquisition of the Sentinel-1 IW image, precipitation occurred on three of the previous five days (March 16, 17 and 19), and the average temperatures were above the water melting point of the snow on three of those days, March 16, 17 and 18. Maximum and minimum temperatures were positive on March 16 and 17. (Table II).

Based on the zones proposed by Paterson (1994), two radar zones were identified in the Sentinel-1 IW radar image (Table III and Figure 3): wet-snow and bare-ice zones. The wet-snow zone is observed in the darkest parts (≤ 13 dB) and covering most of the highest elevation of the icefields. As shown in Table III, other authors have found different values for wet-snow and backscatter from the bare-ice zone.

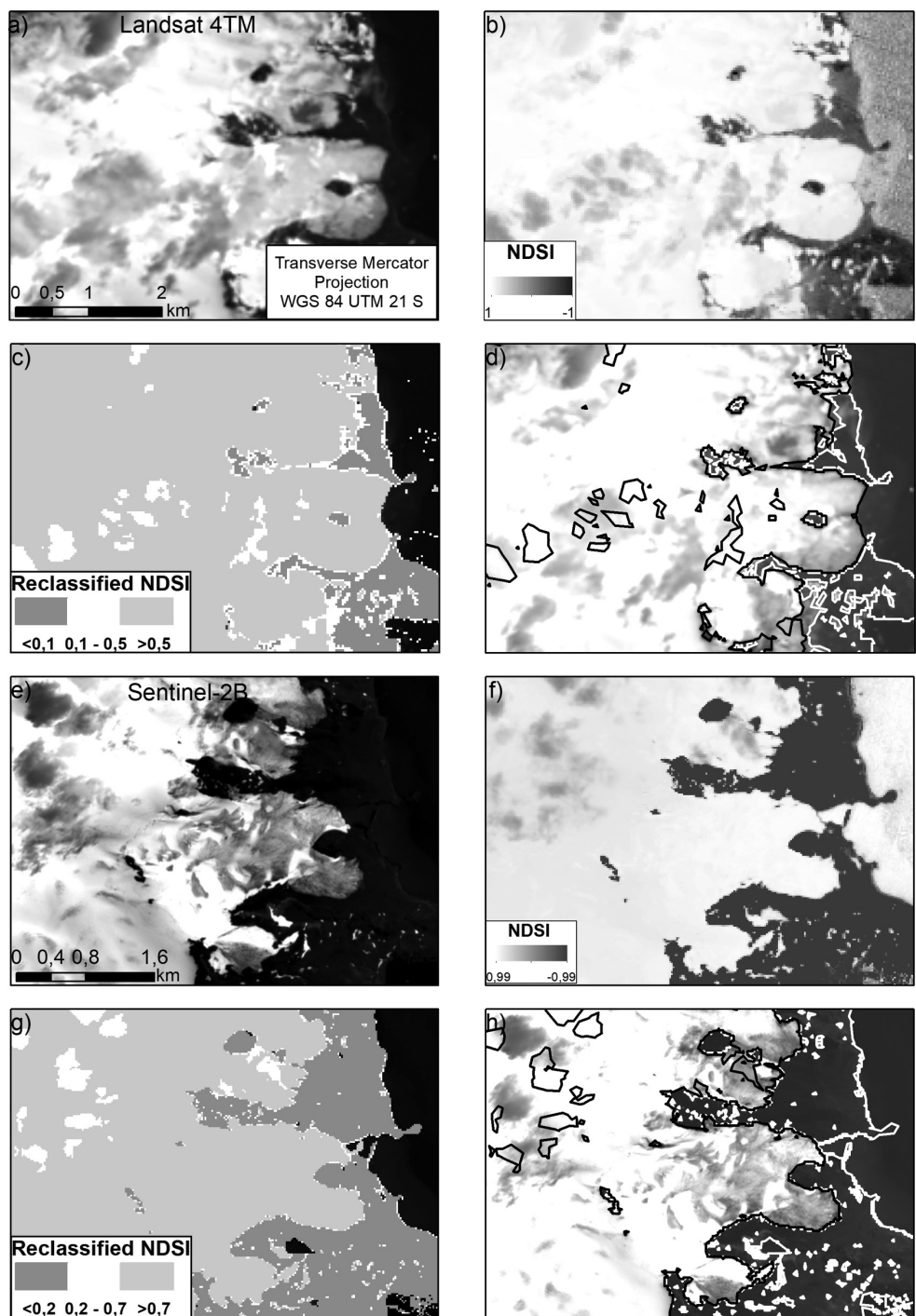


Figure 2. Illustration of the NDSI Classification in the Warszawa Ice Field, a complex area chosen for validation. (a) Landsat 4 TM image (January 28, 1989) in RGB 321 composite showing glacier fronts in contact with ice-free subaerial areas. (b) NDSI classification result showing the values of the stretched targets. (c) Raster reclassified for glaciers using a threshold > 0.5 . (d) Final glacial cover mapping for the L-4 image (after applying the proposed methodology). (e) Sentinel-2 image (January 9, 2020) in RGB 432 composite showing glacier fronts in contact with ice-free subaerial areas. (f) NDSI classification result showing the values of the stretched targets. (g) Raster reclassified for glaciers using a threshold > 0.7 . (h) Final glacial cover mapping for the S-2 image (after applying the proposed methodology).

KGI has an average maximum glacier elevation of approximately 432 m, and more than 55% of the total glacial area of the island (553.78 km²) is located at elevations higher than 300 m. In terms of the total area of TSL altitude (443.04 km²), this corresponds to 44.3% of the total glacial area. The coefficient of determination between the area above TSL altitude and the percentage loss of glacial area was 29.52%, with a negative trend line.

Icefields containing data values for TSL altitude were EP, CP, WI, AI, and KI. Some glaciers in KP and BD did not show attitude TSL because they were either below 300 m in altitude or did

not have the proposed backscatter intervals. The CP has the highest percentage of area above TSL altitude (55%) and a maximum elevation of 726 m. Compared to the other icefields where the TSL altitude was recorded, the WI had the smallest percentage area (29%). The AI had a percentage area of 53%, EP of 40%, and KI had an area of 33%.

Method validation

In the 2020 Sentinel-2B image, the ranges of the NDSI-covered classes (rock, cloud, and glacier) were defined as 0.2 to 0.7 and > 0.7, respectively. The NDWI range denoted the aqueous body

Table II. Climatological data for the Chilean Antarctic station Frei Montalva, including average data for surface air temperature at 2 p.m. for the days preceding the acquisition of the Sentinel-1 radar image.

Frei Montalva Station - Climatological data				
Date	Mean °C	Min. °C	Max. °C	Precipitation
03/16/2020	2.1	1.4	2.9	1.0 mm
03/17/2020	1.1	0.1	2.0	1.2 mm
03/18/2020	-0.5	-3.5	2.6	-
03/19/2020	-2.1	-3.6	-0.5	0.3 mm
03/20/2020	-3.1	-6.2	0	-

Table III. Backscatter intervals for the Bare Ice Zone and the Wet-Snow Zone proposed by different authors in other studies.

Radar zone	Backscattering	Sensor/Type	Polarization	Band	Source
Bare-ice zone	-12 to -10 dB	ERS-1	VV	C	Smith et al. (1997)
	-13 to -10 dB	ERS-2	VV	C	Braun et al. (2000)
	-14 to -6 dB	ERS-1/2	VV	C	Rau et al. (2000)
	-17 to -15 dB	Sentinel-1 / GRD	HH	C	This study
Wet-snow zone	-22 to -6 dB	ERS-1	VV	C	Smith et al. (1997)
	-22 to -15 dB	ERS-2	VV	C	Braun et al. (2000)
	-25 to -15 dB	ERS-1/2	VV	C	Rau et al. (2000)
	< 4 dB	Sentinel-1 / GRD	HH	C	Zhou & Zheng (2017)
	-29.9, -28.54 dB	Envisat/ Sentinel-1 A and B / RADARSAT-2	HH / HH / HH	C	Zhou et al. (2021)
	≥ -13 dB	Sentinel-1 / GRD	HH	C	This study

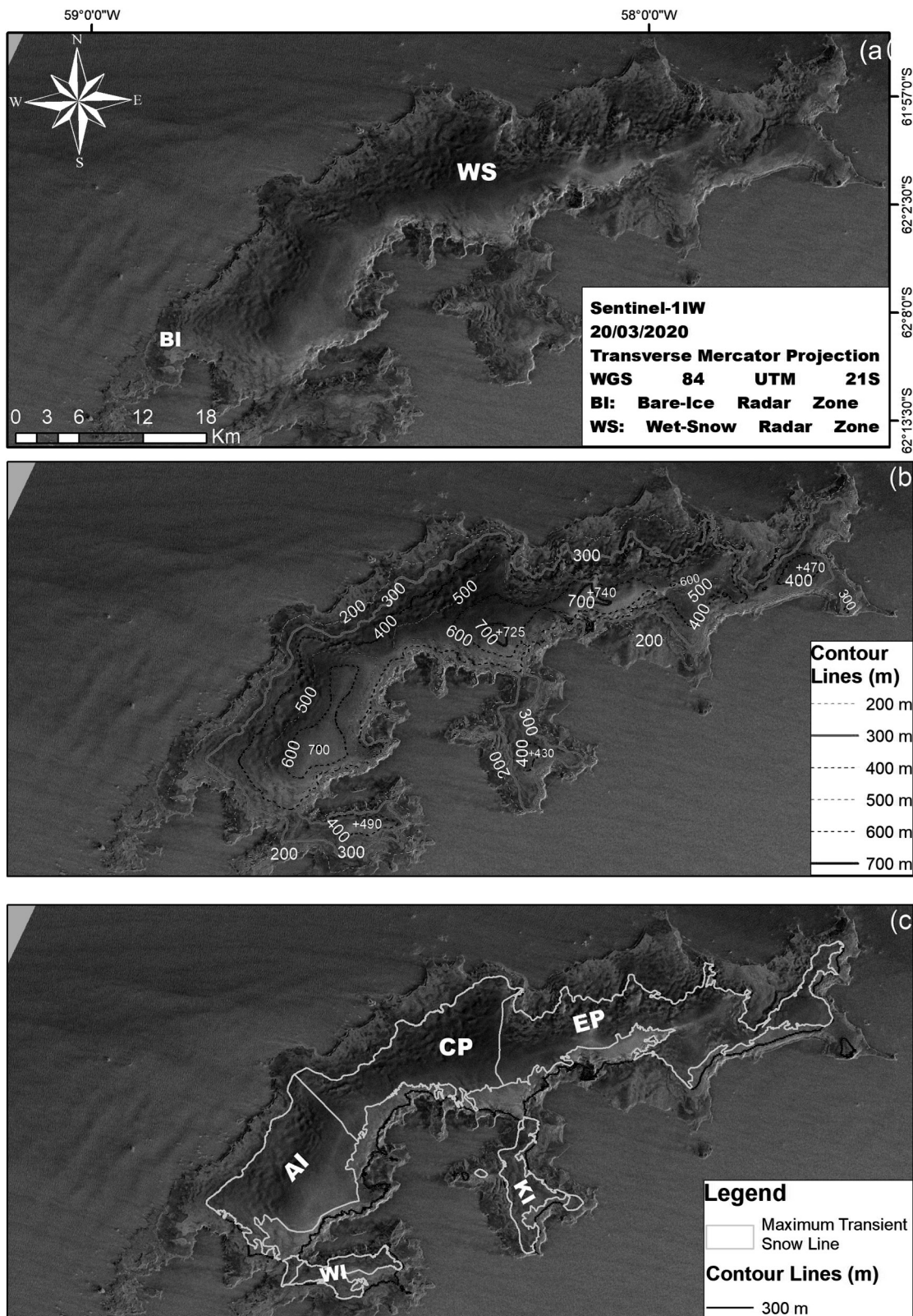


Figure 3. a) Wet Snow (WS) and Bare Ice (BI) zones, b) topographic contour and c) Transient Snow Line identified in 2020 Sentinel-1 IW radar image (summer).

class as values > 0.2. The NDSI ranges for the 1988/89 Landsat-4 TM images were < 0.1 for rock, 0.1 to 0.5 for clouds, and > 0.5, clouds, and glaciers, respectively. For aqueous bodies, the NDWI range was defined as > 0.2. These results are consistent with the findings of other authors, who also reported different values (Table IV).

In 2020, the estimated area covered by glaciers was 999.95 km² compared to 1104.8 km² in 1988/1989. Differences between NDSI-generated and manual vectors were minor (0.6% in 2020 and 0.23% in 1988/1989 for the entire KGI). This may be attributed to the contact areas between the glaciers and rocky features. In the validated area of analysis (WI), the total area estimates for the entire KGI have less than 1% uncertainty. Validation was considered satisfactory when observing the correspondence between the target and control points (Figure 4).

Variation in glacier area and environmental conditions

Total glacial area loss for KGI during the studied period was 101.34 km² (error < 1 km²) when considering the values of the spectral indices and 104.85 km² when considering the manual vectorization (Figure 5). In terms of spectral indices values, glacial area loss showed a 9.15%

decrease in the KGI over 32 years, a rate of 3.17 km² per year.

WI is an icefield that shows a TSL altitude and has the highest percentage of area loss, 15.6%, for the study period. The AI lost 6.3% of its glacial coverage area, KI lost 13%, and EP lost 10.4%. At elevations of up to 25 m, a percentage loss of glacial area was found — 98% for KI and greater than 90% for the other icefields (Figure 6). Concerning the other quotas, WI and BD had the highest percentage losses.

WI showed an 82% loss in elevations between 25-50 m, 51% in 50-75 m, 49% in 75-100 m, 18% in 100-150 m, 10% in 150-200 m, 5% in 200-250 m, and 1.18% in elevations greater than 250 m, which is the only icefield with loss values greater than 1% at this level. In contrast, BD showed 97% loss at elevations < 25 m, and 85%, 69%, 23%, 4%, and 1% for the 25-50 m, 50-75 m, 75-100 m, 100-150 m, and 150-200 m elevations ranges, respectively.

All icefields showed losses at elevations of < 200 m (Figure 6). The average loss for class < 25 m is 96%. For the other quotas (25-50 m, 50-75 m, 75-100 m, 100-150 m, 150-200, 200-250 m, and > 250 m) the values are 63%, 42%, 25%, 8%, 4%, 2% and 0%, respectively. The EP experienced significant losses at elevations of 0-25 m and

Table IV. Reflectance intervals for ice and snow proposed by various authors in other studies, as well as the sensor used.

NDSI value	Sensor	Source
0,4	Landsat TM	Morris et al. (2006)
0,39 e 0,47	Landsat TM	Silverio & Jaquet (2012)
0,59	Landsat TM	Sanches et al. (2015)
0,55 e 0,9	Landsat TM	Rekowsky et al. (2019)
0,2 - 0,67 wet snow zone or water zoner e, 0,67 > snow zone	Sentinel-2	Hillebrand et al. (2018)
0,7 > glacier and snow zone	Sentinel-2B	This study
0,5 > glacier and snow zone	Landsat TM	This study

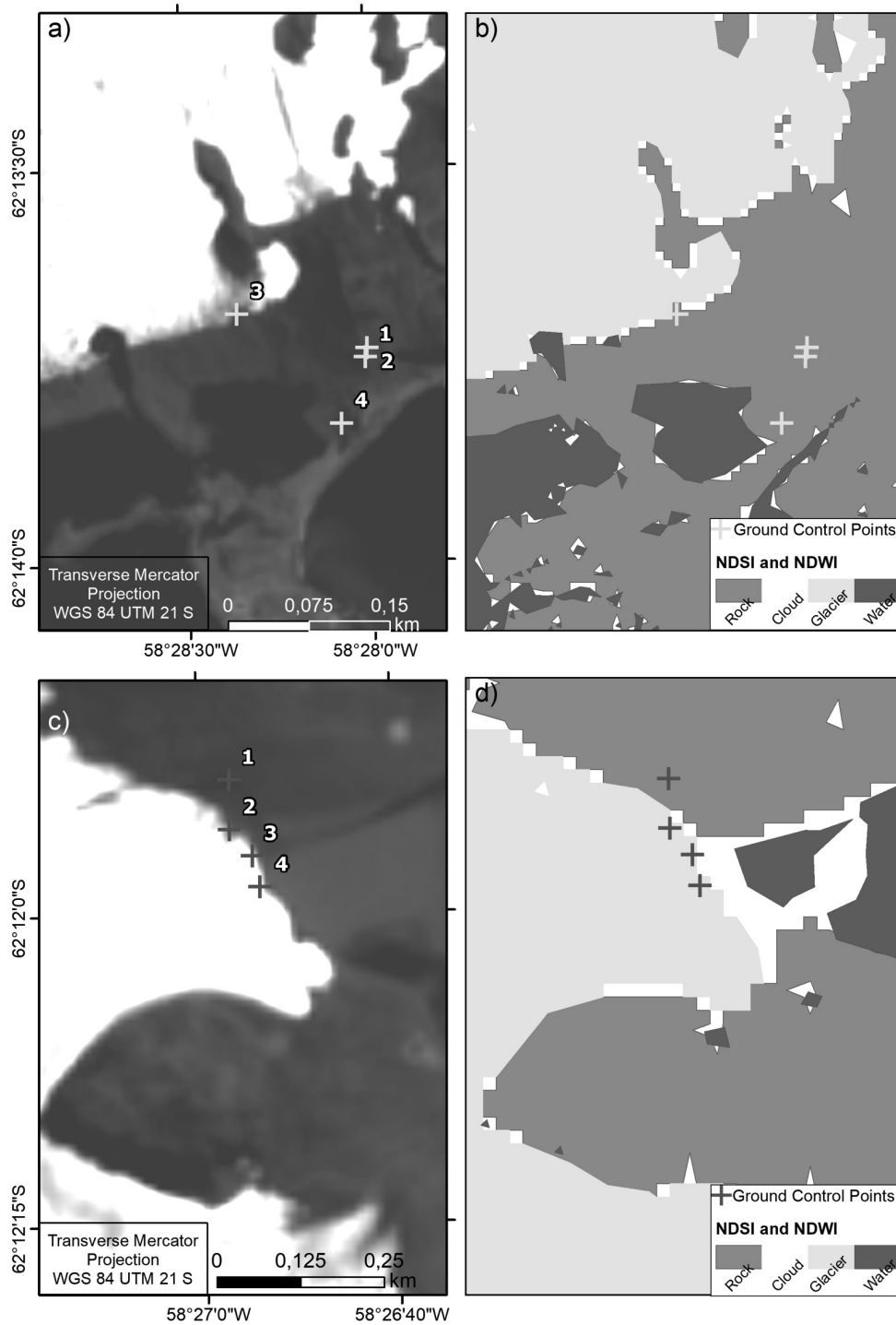


Figure 4. Field control points and the automatic classification obtained by NDSI and NDWI. (a) S-2B image (taken on January 9, 2020) showing the front of Windy Glacier - Windy Mor1 (1); Windy Mor2 (2); Windy Mor3 (3); and Windy Mor4 (4). (b) Field control points and the automatic classification obtained by NDSI and NDWI in the Windy Glacier's front. (c) S-2B image (taken on January 9, 2020) showing the front of Baranowski Glacier - Lateral Moraine (1); Recessional Moraine (2); Bara Sub1 (3); and Subsurface Bara (4). (d) Field control points and automatic classification obtained by NDSI and NDWI in the Baranowski glacier's front. (Control points were obtained by Denni Moraes, during OPERANTAR XXXVIII).

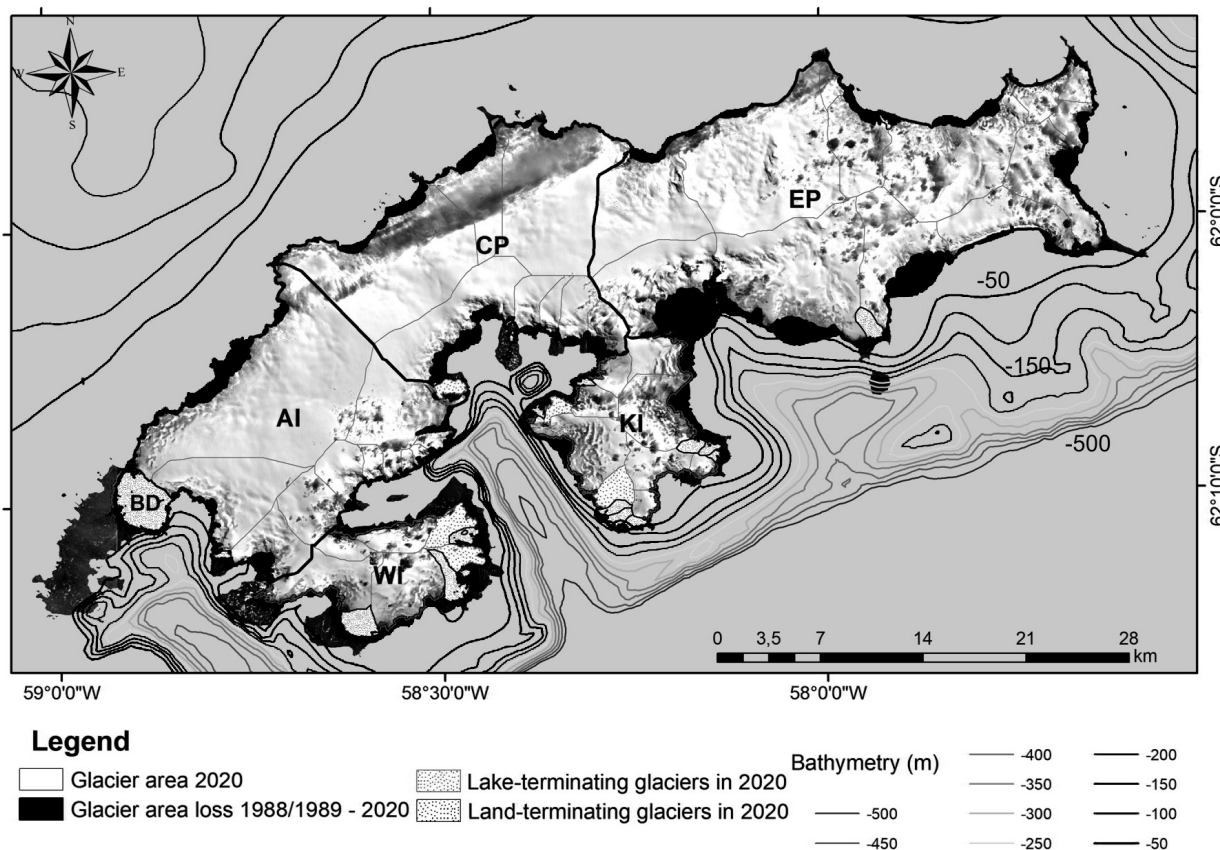


Figure 5. Illustration regarding the loss of area of glaciers, with their respective glacial drainage dividers, from KGI in the years 1988 - 1989 to the year 2020, with differentiation of marine and land-terminating glacier – terrestrial or lacustrine. In addition to the bathymetric lines surrounding the KGI.

25-50 m (97% and 64%, respectively), which was greater than the average percentage loss in both cases. The same pattern was observed for WI and BD.

Figure 7(a) shows a graph of the percentage loss of average area per KGI sector. One may observe that the sector-oriented toward the BS shows higher losses. The glaciers in this sector (58 in total) lost approximately 20.53% of their area during this period. For DP, this value was 9.38%. The Drake sector (13 glaciers) has a greater standard error (0.034), while the BS has a value of 0.025. Figure 7(b) shows the percentage of average area loss in relation to the glacier terminus type in the KGI, including the Collins Glacier.

The atmospheric temperature warming trend is greater in the Bransfield Strait (BS) compared to that of the DP (Figure 8). The winds at 10 m show that V-Winds are relatively slow and U-Winds are relatively fast; consequently, the wind vector will be more influenced by the U-Wind. The 10-meter V-wind anomaly (2011/2019–1979/2010) over the islands appears opposite on the north and south sides, that is, from the south and the north (Figure 8e).

Regarding bathymetry, one of the parameters used to characterize glacier fronts, a steeper topographic profile was observed near the coast in the sector facing the BS. In terms of glaciers with a non-marine terminus, only one facing the DP (ID GLIMS 288746) was observed;

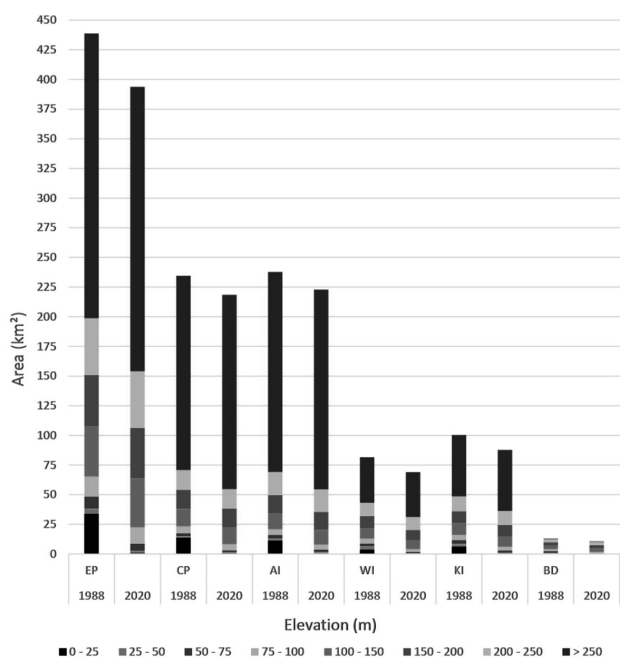


Figure 6. Comparison graph of the ice fields area for the period of analysis, separated by elevation quotas of 0-25 m, 25-50 m, 50-75 m, 75-100 m, 100-150 m, 150-200 m, and > 250 m.

the other glaciers with this feature are either the Collins Glacier (ID GLIMS 288411) in the BD or facing the BS. Compared to the BS's coastal sector (Figure 5), greater distance ranges from bathymetric elevations in the DP represent a smaller topographic amplitude, that is, a smaller slope. The southern sector of the KGI had the greatest variation in elevation. Glaciers in the KP (glaciers without an icefield) and BD have the highest percentages of loss (28.2% and 17.4%, respectively).

Case study - glaciers of the Eastern Part

In the EP, the highest rates of glacial area loss were observed among the icefields with the largest area, which also flowed in the DP, in addition to the AI and CP. Despite having high elevation points (maximum elevation of 739 m), the EP has the lowest percentage of area at elevations above 300 m (50.7%). In contrast,

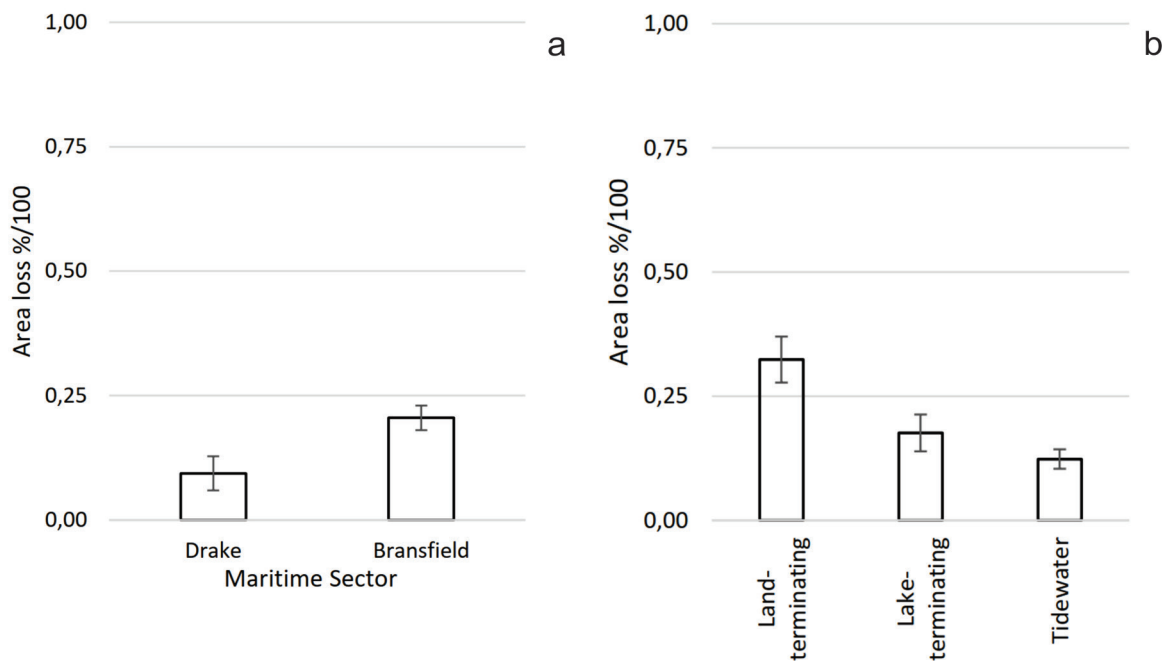


Figure 7. (a) Graph of the percentage of average area loss of the KGI glaciers by sector and the standard error for the analysis sample, excluding the Collins glacier, which is located in the BD. (b) Graph of the percentage of average area loss of the KGI glaciers by terminus type, land-, lacustrine- or marine-terminating, as well as the standard error for the sample, which included all glaciers in the study area.

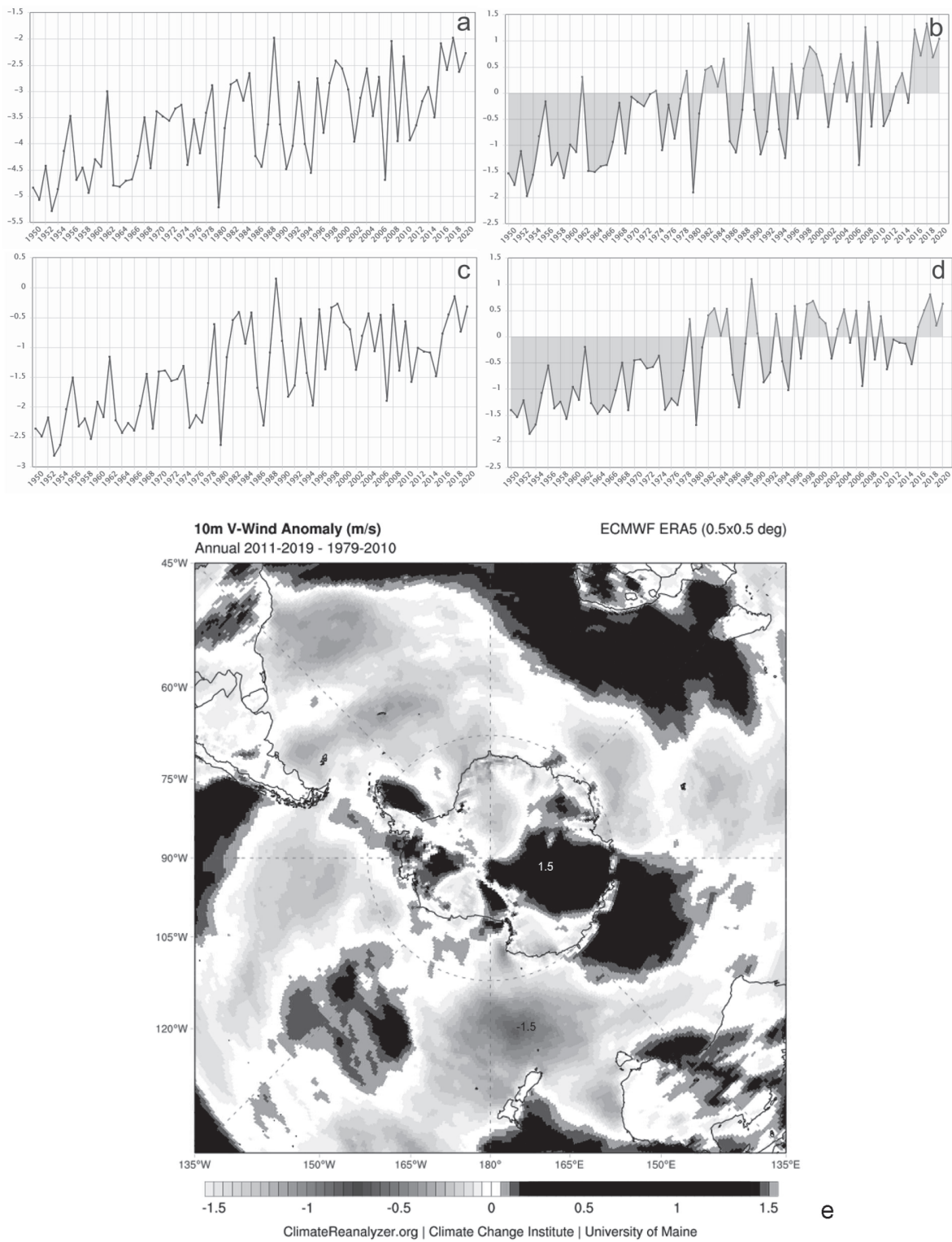


Figure 8. a) Annual 2m Temperature ($^{\circ}\text{C}$) and b) Annual 2m Temperature ($^{\circ}\text{C}$) anomaly in Bransfield Strait sector near at the KGI in period 1950-2020; c) Annual 2m Temperature ($^{\circ}\text{C}$) and d) Annual 2m Temperature ($^{\circ}\text{C}$) anomaly in Drakes Passage sector (just north of the islands) in period 1950-2020; e) Mean 2011-2019 V-Winds minus 1979-2010 Average.

the CP and AI values for the same were 67% and 65.4%, respectively.

Glaciers facing BS, such as Poland Piedmont (ID GLIMS 287457) and Hektor Icefall A (ID GLIMS 288875), demonstrated high area loss values of 37.4% and 53.7% of percentage area above TSL altitude, respectively. In terms of bathymetry, these are glaciers that have a short distance from the -15 meters curve (Figure 9).

Smaller losses and a greater distance from the bathymetric curve of -15 m were observed for glaciers facing the DP, such as Eldred (ID GLIMS 287732), and Drake (ID GLIMS 289750). Eldred Glacier still has 75.2% of its area above the TSL elevation. The coefficient of determination between the bathymetric distance from the glacial margin to depths greater than 15 m and glacial area loss was 27.15%. The trend line was negative.

DISCUSSION

Potentials and limitations of glacier monitoring methodology and data

Potentials and limitations of radar zones identification

In terms of the association with glacier zones, a wet-snow radar zone comprising the accumulation portion and a bare ice radar zone in the ablation area could be identified. When using the C band, the backscatter values resulting from glacier radar zones vary depending on the author and date of the analysis, as evidenced by other studies. For wet-snow zones in the ablation season, Smith et al. (1997) discovered values ranging from -22 to -6 dB (initial melting snowpack, metamorphosed and roughened melting snow surfaces), and Braun et al. (2000) obtained for KGI intervals of -22 to -15 dB. These

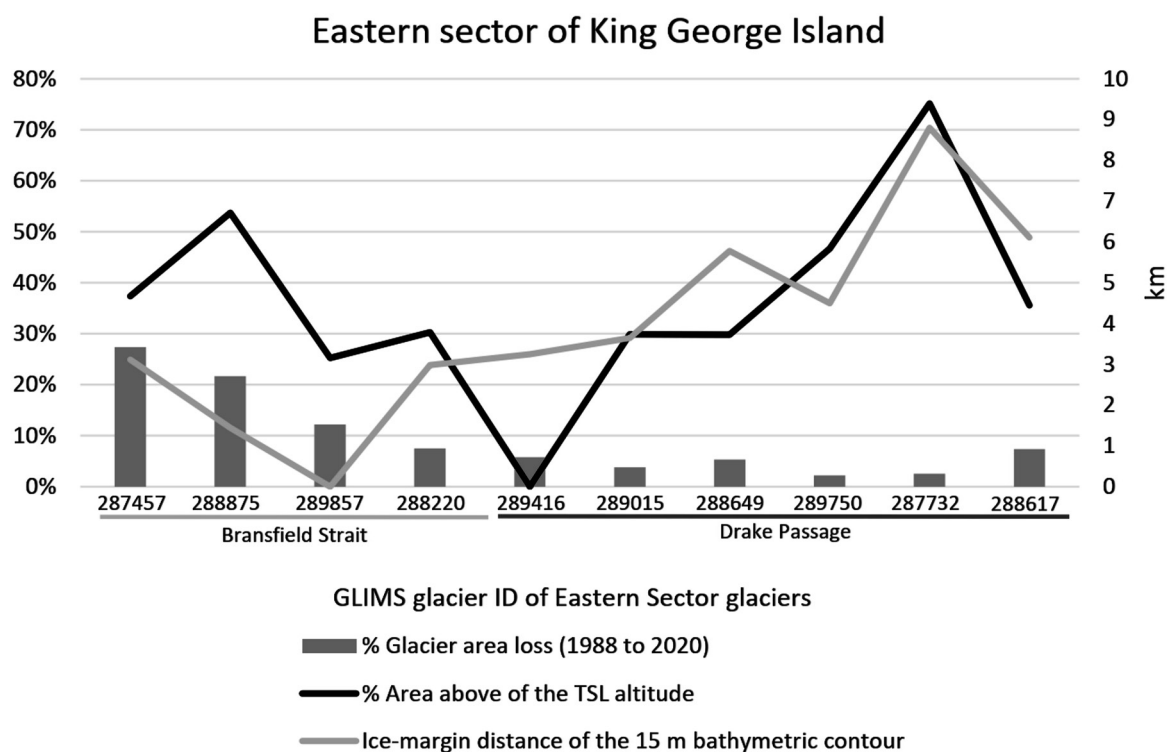


Figure 9. Graph of glaciers in the Eastern Part, excluding those that face Destruction Bay and those that end on land. The percentage area loss information for the analysis period is shown in bars, the percentage area above TSL altitude in black, and in gray is shown the distance in kilometers from the glacier margin to bathymetric elevations equal to or greater than 15 meters depth.

dissimilarities can be for the difference in the region analyzed in both studies (icefield in British Columbia and KGI). The backscatter values of ≤ -13 dB obtained in our study may be associated with the presence of water, as wet snow absorbs more radiation (Zhou & Zheng 2017). This image context is inferred by the distribution of positive temperature and precipitation averages in the days preceding image acquisition. It is worth noting that interpreting radar images in conjunction with meteorological data is recommended for future studies involving Maritime Antarctica, as it aids in understanding the image backscatter variation.

In the bare ice zone, there are larger differences between the backscatter values observed in our study and those found by Smith et al. (1997) (-12 to -10 dB) and Braun et al. (2000) (-13 to -10 dB). This may be attributed to the use of different sensors for target identification and also for the difference in the polarization. Backscatter from ice or water is affected by the radar wavelength, polarization, and angle of incidence (Mäkynen et al. 2002). The incidence angle of the Sentinel-1 IW image is 20-45 degrees, which modifies the feedback signal measurement. Higher incidence angles exhibit changes in backscatter due to the characteristics of the ice column (Atwood et al. 2015).

Furthermore, backscatter value thresholds for bare ice and wet-snow zones were not uniform across all glaciers because of the surface roughness factor. This factor is relevant for the analysis of the results, as demonstrated by Lewis & Henderson (1998). As observed in the icefield, glacier points with varying slopes produce different radar signal responses. This same occurrence is observed in the roughness of the crevasse sectors in glaciers, which are generally located towards its terminus.

Potentials and limitations of using spectral indices

The application of spectral indices (NDSI and NDWI) in the region under analysis proved to be effective for delimitation of glacial areas and features. The indices results were comparable to the results obtained manually and considered satisfactory according to the methodology proposed by Albert (2002). According to Pudetko et al. (2018), given the current trend in developing satellite observation systems, high-resolution data (spatial, spectral, and temporal) will be easily available for polar regions in the near future, promoting glacier monitoring. It is noteworthy that the results of this current research contribute to the consolidation of semi-automatic glacier front mapping methods and techniques for other areas of Maritime Antarctica.

The existence of errors and uncertainties may result from pixels relating to boundary zones. The spectral mixtures of different targets may also contribute to error and uncertainty (Shimabukuro & Smith 1991). For example, one of the icefield control points in the study area is near the exit of a subglacial channel. This may affect the spectral response because of the greater humidity in the area.

Changes in KGI glacial cover and the formation of new ice-free areas resulting from glacier outline elevation

In 2020, the KGI presented a lower percentage of glacial coverage area (80.5%) when compared to the area found in 1996/97 (93%) by Braun & Rau (2000). These findings show that the glacier area on the island has continued to decrease over the last few decades. This is in agreement with reported observations from analyses in several studies conducted on the island in the years preceding 2020 (Arigony-Neto et al. 2001,

Rückamp et al. 2011, Rosa et al. 2015a, b, Simões et al. 2015, Pudełko et al. 2018, Sziło & Białik 2018, Perondi et al. 2019, 2020, Oliveira et al. 2019, Petsch et al. 2020).

The rate of glacial area loss (3.2 km²/year) in 1988-2020 period shows good agreement with the findings of the climate series analysis, which include regional warming trends between 1948 and the first decade of the 21st century. Research concerning the regional warming trends includes Braun & Goßmann (2002) and Turner et al. (2005a), as well as the resumption of regional warming identified by Carrasco et al. (2021). This region has also seen an increase in the number of days with liquid precipitation and snow since the 1950s (Turner et al. 2005b) and an increase in the number of days with positive temperatures (Turner et al. 2021).

Approximately 30% of the KGI being located at elevations less than 250 m (Braun & Rau 2000). The study data indicate that areas with the greatest glacial loss are those located at elevations ≤ 250 m. These areas account for 97% of the area showing glacial losses. This scenario is especially concerning for glaciers situated at lower elevations; for example, the Collins - BD glacier has a maximum elevation of 270 m. In this bias, Rückamp et al. (2011) note that if the current rates of atmospheric warming continue, this glacier will disappear in approximately 285 years.

If this glacial area loss scenario is maintained, new ice-free areas may appear in icefields at higher elevations, such as the EP. This is due to higher retreat rates in this icefield. Furthermore, the EP has 49.3% of its area at elevations less than 300 m.

Differences in the behavior of Icefield terminus and the influence of local environmental factors

Elevation and TSL altitude as conditioning factors

Regarding the elevation obtained for the TSL, it was verified by comparison to other authors: Jiahong et al. (1998) defined the TSL at altitudes of 140-150 m a.s.l. for the period 1985-1992; Simões et al. (1999) identified the TSL at altitudes of 300-350 m in 1988 using the SPOT sensor; Braun et al. (2000) documented the TSL in 1996/97 at altitudes close to 250 m a.s.l. using the ERS-2 SAR sensor, and Falk et al. (2018) observed the equilibrium line altitude at an altitude of 260±20 m for 2010-2015 using the SPOT-4 sensor.

Glacial area loss occurred in all icefields, with the KI and WI showing the highest percentage area losses at elevations > 150 m. However, the greatest observed losses occur in low-elevation and/or with no area above the TSL elevation of the Icefields. As a result, it is understood that these factors are related to the loss of glacial area verified for the island.

The percentage of the glacial area above the TSL altitude is related to the glacial area loss for all KGI glaciers. Thus, as previously stated by Bakke & Nesje (2011), the greater the percentage of the area above the TSL elevation, the smaller the loss of glacial area. Regarding the association of glacier maximum elevations, the higher the glaciers, the smaller the loss of area.

The EP had a lower proportion of areas above elevations of 300 m than the AI and CP. These differences can be explained by higher ice discharge in sectors facing the fjords and BS, primarily influencing the losses of the EP, which has more glaciers facing the south sector of the island (fjords and BS) than the AI and CP. Elevation variations were greater in BS than in DP. Braun & Goßmann (2002) highlighted that

the slopes on the north and northwest coasts are gentler, in contrast to the steeper slopes of the shores to the south of the island.

One of the EP glaciers (ID GLIMS 289416) did not have an area above the TSL elevation and had a low percentage area loss (5.62%); this glacier had the smallest size of any glacier in the EP sample. Osmanoglu et al. (2013) identified glacier flow velocities. While the authors use different glacial drainage dividers, it is noted that the region in which this glacier (ID GLIMS 289416) is located has lower flow velocity rates.

Nonetheless, elevation errors in the digital elevation model (DEM) result in errors and uncertainties in the minimum values of the TSL elevation in some areas of the study area, which coincide with sectors of greater slope and possibly with the presence of crevasses. Therefore, it is critical to use DEM that has been digitally processed to correct elevation inconsistencies caused by the generation and acquisition method.

Land-terminating glaciers retreat

Over the past 50 years, large areas along the southern coast of the KGI have lost their permanent ice cover, as noted in the ERA-5 data, which revealed a stronger warming trend for the BS. As a result, several new nunataks emerged, demonstrating a significant reduction in glacier thickness (Pudetko et al. 2018). Land-terminating glaciers showed a 10.62 km² of glacial retraction between 1988/1989-2020. As observed by Perondi et al. (2020) in 2019, a change of 25% of the area of land-terminating glaciers occurred in the last two decades. There was 3.24 km² area loss in the temporal analysis of water-terminating (lacustrine environment) glaciers.

Area loss in land-terminating glaciers (including water-terminating glaciers) creates new ice-free areas and imposes new environmental dynamics and configurations

on the environment, making it vulnerable to paraglacial activity (Ballantyne 2002). According to Rosa et al. (2021), there was a 316% increase in the area of glacial lakes between 1988 and 2000/03, and a 103% increase between 2000/03 and 2020. Petsch et al. (2019) stated that the Fildes peninsula may see an increase in moss fields due to the retreat of the Collins Glacier and the emergence of new proglacial areas. Therefore, glacier monitoring in KGI is essential for understanding the hydrological and geomorphological processes that occur in ice-free portions.

Cook et al. (2014) observed that smaller glaciers respond faster to atmospheric temperature changes and, as also evidenced by this study, Braun & Goßmann (2002) noted higher percentage losses for land-terminating glaciers in Admiralty Bay because of their smaller dimensions. Land-terminating glaciers are sensitive to changes in the mean surface air temperature (Davies et al. 2014), as observed in the KGI.

Retreat of marine-terminating glaciers and their conditions

As marine-terminating glaciers respond both to atmospheric and oceanic forcing, their responses are conditioned by a greater variety of factors, resulting in increasing dynamics. Thus, comprehending their behavior denotes a broader range of conditions. Marine-terminating glaciers in KGI face two distinct sectors, the BS and the DP, which subject them to different conditions as a result of bathymetry and ocean currents.

Moffat & Meredith (2018) classified the BS as having steep and deep bathymetry and mentioned the influence of the CDW in some parts of the strait. According to Llanillo et al. (2019), CDW intrusion from the BS may occur in Maxwell Bay. Therefore, the CDW current is a factor

that should be better understood for the region, because it can influence a greater percentage of area losses in the marine-terminating glaciers facing the BS. This is because the CDW current brings relatively warmer water. Glaciers in this sector may be subject to greater anchorage depth from the front.

Both sectors influence the EP. It has the largest glacial area and faces both DP and BS sectors. There are more open bays in the sector facing the BS (King George Bay and Sherratt Bay) and a more significant influence of water originating from the BS. While the other icefields connected to the two sectors, CP and AI, flow to fjords in the sector facing the BS and have lower percentage area losses (6.9% and 6.3%) than the EP.

Another icefield linked to King George Bay is the KI, which presented the highest percentage loss of glacial area for elevations of up to 25 m. These losses can be explained by the retreat of the Anna Sul glacier, which faces this bay and interacts more with the BS than other glaciers that face inlets and bays, such as Martel Cove and Admiralty Bay. Thus, the ocean-glacier linkage triggers the Ana Glacier terminus change.

Several studies have shown that the trend of rising atmospheric air temperatures in recent decades is related to the loss of sea ice and that rising ocean temperatures can lead to more significant basal melting of outlet glaciers, affecting the dynamics of thickness, retreat, and mass loss (Reeh et al. 2001, Rignot et al. 2001, Rignot & Steffen 2008). Low sea ice concentrations in the AP may also be associated with an increased negative mass balance for glaciers in this region (Hillebrand et al. 2021). SAM is also an influencing factor, as it causes oceanic and atmospheric warming of the western part of the AP (Marshall et al. 2006). Understanding the role of sea ice in the KGI as indicated by Simões et al. (1999) for both the BS

and DP sectors and its implications for sector dynamics is still necessary.

Another distinction between glaciers in these two sectors is the difference in thickness. According to Osmanoğlu et al. (2013), glaciers facing the BS, particularly those in Admiralty Bay and the KI, have smaller snout thicknesses than those facing the DP sector. In the same study, the authors presented glacier ice-flow velocity values, where a large portion of this discharge originates from glaciers facing the DP, except for two glaciers facing King George Bay and the Lange Glacier.

Regarding of area loss, it is inferred that, in addition to the influence of the area of the icefield that is located above the TSL altitude, bathymetry also has a role in the area loss of marine-terminating glaciers, as this will affect the point of anchorage of glaciers. The EP marine-terminating glaciers facing the DP are subject to shallower conditions than those facing the BS. The largest percentage of area losses was found in the sector facing the BS (Figure 7).

This scenario is observed through the regularity between the percentage area loss ratio and the bathymetric distance below -15 meters in EP. This relationship has a negative slant, indicating that as the distance between the glacier front increases and for depths greater than -15 m, the loss of the glacier area will decrease. This relationship reiterates the observations made by Braun & Goßmann (2002), who identified greater glacial loss among marine-terminating glaciers for those that had anchorage at greater depths in the fjord.

Variations in the depth of the glaciomarine environment and its impact on the retreat rate and dynamic of the glaciers were also identified by Hill et al. (2018) in northern Greenland and by other authors in many other regions of Greenland (Thomas et al. 2009). These authors demonstrated that glaciers anchored in deeper

marine sectors shrink more than those anchored in shallower sectors due to increased basal and lateral friction, which influences calving rates.

It is worth noting that, as Braun & Goßmann (2002) indicate, not all glaciers respond similarly to changes in the environment observed over time. When these authors examined the decades before 2000, they observed that some glaciers, such as Lange (AI) and Viéville (KI), have higher retreat rates than others, which remained more stable on the island. Our research found glaciers with higher retreat rate, such as Ana (ID GLIMS 287457) and ID GLIMS 289857, which are linked to the EP. These substantial retreats can be attributed to the dynamics of the glacier tongue adjusting to a stable position (Braun & Goßmann 2002). Greater water depths in floating ice tongue, for example, contribute to greater calving rate, whereas moraines and bed topography contribute to greater stability of the floating ice tongue (Braun & Goßmann 2002).

The KGI outcomes were consistent with the findings of other surveys. When analyzing two glaciers in the AP, Simões et al. (2020) concluded that the combination of slope, area, elevation, and orientation, or even the change in the terminus (such as the loss of floating platforms) promoted different sensitivities of glaciers to climate change. Differences in glacier behavior can be attributed to differences in their local climates, orientation, size, slope, and individual dynamic (Nesje 1992, Casassa et al. 1997, Harrison & Winchester 1998). Furthermore, the effect of climatic fluctuations on glacier mass balance has been determined by the glacier area-altitude distribution (Nesje & Dahl, 2000). Although the mechanism of glacier retreat is complex, some causes are discussed and presented in this research.

CONCLUSIONS

Retreats observed in the icefields are a response to the climatic variables acting in the KGI and other factors that operate by modulating the behavior of glacier fronts, which explain differences in retreat and TSL altitude found in each icefield. Glacial area losses were observed for all KGI glaciers, with the magnitude of the losses varying according to the glacier terminus type and sector location.

The use of remote sensing has evidenced recent changes in the KGI icefields since 1988. Short-term glacier area changes, maximum elevation, snowline altitude, thickness, and the presence of the land-terminating glacier terminus vary between the BS and the DP. These contrasts result from regional climatic variations and reveal glacier geometry dependence.

Based on the results obtained and the verification of environmental changes previously identified by other authors, the issue of basin limits must be reviewed. For future studies, mappings with greater temporal details of the investigated region will be relevant.

Differences in TSL altitude, the thickness of the floating ice tongue, and water depth near the glacier terminus are all important factors to consider when generating glacier shrinkage scenarios. Future studies may investigate factors that influence mass loss, such as surface melting and even accumulation, such as snow precipitation. In addition, the role of CDW and sea ice in the area and their interactions with the outlet glaciers.

Acknowledgments

We acknowledge Jeffrey Auger and Maria Eliza Sotille for assistance in language editing. We also acknowledge the Conselho Nacional de Desenvolvimento Científico e Tecnológico (CNPq) Project 465680/2014-3 (INCT da Criosfera); Coordenação de Aperfeiçoamento de Pessoal de Nível Superior (CAPES); Brazilian Antarctic Program (PROANTAR); Foundation of Research Support

of the State of Rio Grande do Sul (FAPERGS) for financial support; Pró-reitoria de Pesquisa of UFRGS (PROPESQ) and Programa de Pós-Graduação em Geografia of UFRGS.

REFERENCES

- ALBERT TH. 2002. Evaluation of Remote Sensing Techniques for Ice-Area Classification Applied to the Tropical Quelccaya Ice Cap, Peru. *Polar Geogr* 26: 210-226.
- AQUINO FE, SETZER A & SIMÕES JC. 2006. The sub-antarctic atmospheric circulation between 15°W and 90°W and its effects on the climates of the Antarctic Peninsula and southern South America. In: Antarctic Peninsula climate variability: observations, models and plans for IPY Research, University of Colorado, Boulder, Colorado, EUA, p. 19.
- ARIGONY-NETO J, SIMÕES JC, BREMER UF & AQUINO FE. 2001. Detecção de Mudanças Ambientais na Antártica através de Dados de Sensoriamento Remoto e Mapas Históricos. *Pesq Geoci* 28: 337-342.
- ATWOOD DK, GUNN GE, ROUSSI C, WU J, DUGUAY C & SARABANDI K. 2015. Microwave Backscatter from Arctic Lake Ice and Polarimetric Implications. *IEEE Trans Geosci Remote Sens* 53: 5972-5982.
- BAKKE J & NESJE A. 2011. Equilibrium-Line Altitude (ELA). In: Singh VP, Singh P & Haritashya UK (Eds), *Encyclopedia of Snow, Ice and Glaciers*. Dordrecht: Springer, p. 268-276.
- BALLANTYNE CK. 2002. Paraglacial geomorphology. *Quat Sci Rev* 21: 1935-2017.
- BARBOZA HC, BORTOLI AL, SIMÕES JC, CUNHA RD & BRAUN M. 2004. Bidimensional numerical simulation of the Lange Glacier, King George Island, Antarctica: preliminary results. *Pesq Antart Bras* 4: 67-76.
- BLINDOW N, SUCKRO SK, RÜCKAMP M, BRAUN M, SCHINDLER M, BREUER B, SAURER H, SIMÕES JC & LANGE MA. 2010. Geometry and thermal regime of the King George Island ice cap, Antarctica, from GPR and GPS. *Annals of Glaciology* 51(55): 103-109.
- BOZKURT D, BROMWICH DH, CARRASCO J, HINES KM, MAUREIRA JC & RONDANELLI R. 2020. Recent near-surface temperature trends in the Antarctic Peninsula from observed, reanalysis and regional climate model data. *Adv Atmos Sci* 37: 477-493.
- BRAUN M & GOßMANN H. 2002. Glacial changes in the areas of Admiralty Bay and Potter Cove, King George Island, Maritime Antarctica. In: Beyer L et al. (Eds), *Geoecology of Antarctic ice-free coastal landscapes*, Berlin, Heidelberg: Springer, p. 75-89.
- BRAUN MH & RAU F. 2000. Using a multi-year data archive of ERS SAR imagery for the monitoring of firn line positions and ablation patterns on the King George Island ice cap (Antarctica). *Proceedings of EARSeL-SIG-Workshop Land Ice and Snow*. Dresden, Germany 1: 281-291.
- BRAUN MH, RAU F, SAURER H & GOßMANN H. 2000. Development of radar glacier zones on the King George Island ice cap, Antarctica, during austral summer 1996/97 as observed in ERS-2 SAR data. *Ann Glaciol* 31: 357-363.
- BRAUN MH, BETSCH T & SEEHAUS T. 2016. King George Island TanDEM-X DEM, link to GeoTIFF. PANGAEA. Available in: <https://doi.pangaea.de/10.1594/PANGAEA.863567> Access in: 18/11/2020.
- CARRASCO JF. 2013. Decadal changes in the near-surface air temperature in the western side of the Antarctic peninsula. *Sci Res J* 3: 275-281.
- CARRASCO JF, BOZKURT D & CORDERO RR. 2021. A review of the observed air temperature in the Antarctic Peninsula. Did the warming trend come back after the early 21st hiatus? *Polar Sci* 28: 100653.
- CASASSA G, BRECHER H, RIVERA A & ANIYA M. 1997. A century-long recession record of Glaciar O'Higgins, Chilean Patagonia. *Ann Glaciol* 24: 106-110.
- CONGEDO L. 2016. Semi-Automatic Classification Plugin Documentation. Release 6.0.11. Available in: <DOI:10.13140/RG.2.2.29474.02242/1>. Access in: 18/11/2021.
- COOK AJ, FOX AJ, VAUGHAN DG & FERRIGNO JG. 2005. Retreating glacier fronts on the Antarctic Peninsula over the Past Half-Century. *Science* 308: 541-544.
- COOK AJ, HOLLAND PR, MEREDITH MP, MURRAY T, LUCKMAN AJ & VAUGHAN DG. 2016. Ocean forcing of glacier retreat in the western Antarctic Peninsula. *Science* 353: 283-286.
- COOK AJ, VAUGHAN DG, LUCKMAN AJ & MURRAY T. 2014. A new Antarctic Peninsula glacier basin inventory and observed area changes since the 1940s. *Antarct Sci* 26: 614-624.
- DA ROSA CN, BREMER UF, PEREIRA FILHO W, SOUSA JÚNIOR MA, KRAMER G, HILLEBRAND FL & JESUS JB. 2020. Freezing and thawing of lakes on the Nelson and King George Islands, Antarctic, using Sentinel 1A synthetic aperture radar images. *Environ Monit Assess* 192: 559.
- DAVIES BJ, CARRIVICK JL, GLASSER NF, HAMBREY MJ & SMELLIE JL. 2012. Variable glacier response to atmospheric warming, northern Antarctic Peninsula, 1988-2009. *The Cryosphere* 6: 1031-1048.
- DAVIES BJ, GOLLEDGE NR, GLASSER NF, CARRIVICK JL, LIGTENBERG SRM, BARRAND NE, BROEKE MR, HAMBREY MJ & SMELLIE JL. 2014. Modelled glacier response to centennial temperature

and precipitation trends on the Antarctic Peninsula. *Nature Clim Change* 4: 993-998.

DOZIER J. 1984. Snow reflectance from Landsat-4 Thematic Mapper. *IEEE Trans Geosci Remote Sens* 22: 323-328.

DOZIER J. 1989. Spectral signature of alpine snow cover from the landsat thematic mapper. *Remote Sens Environ* 28: 9-22.

EDWARDS TL ET AL. 2021. Projected land ice contributions to twenty-first-century sea level rise. *Nature* 593: 74-82.

EUROPEAN SPACE AGENCY. 2021. Sentinel User Guides. Available in: <<https://sentinels.copernicus.eu/web/sentinel/home>>. Access in: 20/05/2021.

FALK U, LOPEZ D & SILVA-BUSSO A. 2018. Multi-year analysis of distributed glacier mass balance modelling and equilibrium line altitude on King George Island, Antarctic Peninsula. *The Cryosphere* 12: 1211-1232.

FATRAS C, FERNANDEZ-PALMA B & MARTILLO C. 2020. Estimating ice retreat on Greenwich Island - Antarctica between 1956 and 2019 using optical and SAR imagery. *Polar Sci* 24:100526.

FERRON FA, SIMÕES JC, AQUINO FE & SETZER AW. 2004. Air Temperature Time Series for King George Island, Antarctica. *Braz Antarct Res* 4: 155 - 169.

GERRISH L, FRETWELL P & COOPER P. 2020. High resolution vector polylines of the Antarctic coastline (7.3) UK Polar Data Centre, Natural Environment Research Council, UK Research & Innovation. Available in: <https://www.scar.org/resources/antarctic-digital-database/>. Access in: 18/11/2021.

GJERMUNDSEN EF, MATHIEU R, KAAB A, CHINN T, FITZHARRIS B & HAGEN JO. 2011. Assessment of multispectral glacier mapping methods and derivation of glacier area changes, 1978-2002, in the central Southern Alps, New Zealand, from ASTER satellite data, field survey and existing inventory data. *J Glaciol* 57: 667-683.

GLIMS. 2000. Global Land Ice Measurements from Space. Available in: <http://www.glims.org/> Access in:15/01/2021.

HALL DK, BENSON CS & FIELD WO. 1995a. Changes of glaciers in glacier bay, Alaska, using ground and satellite measurements. *Phys Geogr* 16: 27-41.

HALL DK, RIGGS GA & SALOMONSON, VV. 1995b. Development of methods for mapping global snow cover using moderate resolution imaging spectroradiometer data. *Remote Sens Environ* 54: 127-140.

HARRISON S & WINCHESTER V. 1998. Historical fluctuations of the Gualas and Reicher Glaciers, North Patagonia Icefield, Chile. *Holocene* 8: 481-485.

HILL EA, CARR JR, STOKES CR & GUDMUNDSSON GH. 2018. Dynamic changes in outlet glaciers in northern Greenland from 1948 to 2015. *The Cryosphere* 12: 3243-3263.

HILLEBRAND FL, ROSA CN & BREMER UF. 2019. Mapeamento das zonas de neve úmida e de percolação por meio do Sentinel-2. *Anuário IGEO* 41: 96-103.

HILLEBRAND FL, BREMER UF, ARIGONY-NETO J, ROSA CN, JESUS JB, IDALINO FD & SAMPAIO MIR. 2021. Influência das fases do SAM na distribuição espacial do gelo marinho na região norte da Península Antártica. *Rev. Brasileira de Geomorfologia*, [s. l.], v. 22, n. 1, p. 187-201.

HOCK R & HUSS M. 2021. Glaciers and climate change. In: Letcher TM (Ed), *Climate Change, observed impacts on planet Earth*. Amsterdam: Elsevier, p. 157-176.

HOWAT IM, PORTER C, SMITH BE, NOH MJ & MORIN P. 2019. The Reference Elevation Model of Antarctica. *The Cryosphere*, 13, 665-674.

HUGONNET R, MCNABB R, BERTHIER E, MENOUNOS B, NUTH C, GIROD L, FARINOTTI D, HUSS M, DUSSAILANT I, BRUN F & KAAB A. 2021. Accelerated global glacier mass loss in the early twenty-first century. *Nature* 592: 726-731.

IPCC - INTERGOVERNMENTAL PANEL ON CLIMATE CHANGE. 2021. *Climate Change 2021. The Physical Science Basis. Climate Change 2013: The Physical Science Basis. Contribution of Working Group I to the Fifth Assessment Report of the Intergovernmental Panel on Climate Change*. Suíça. Available in: Sixth Assessment Report (ipcc.ch). Access in: 09/12/2021.

JIAHONG W, JIANCHENG K, JIANKANG H, ZICHU X, LEIBAO L & DALI W. 1998. Glaciological studies on the King George Island ice cap, South Shetland Islands, Antarctica. *Ann Glaciol* 27: 105-109.

KEJNA M, LÁSKA K & CAPUTA, Z. 1998. Recessión of the Ecology Glacier in the period 1961 - 1996. In: Glowacki B (Ed), *Polish Polar Studies. 25th International Polar Symposium, Warszawa*, p. 121-128.

KEJNA M. 1999. Air temperature on King George Island, South Shetland Islands, Antarctica. *Pol Polar Res* 20: 183-201.

KEJNA M, ARAZNY A & SOBOTA I. 2013. Climatic Change on King George Island in the Years 1948 - 2011. *Pol Polar Res* 34: 213-235.

KING JC & HARANGOZO SA. 1998. Climate change in the western Antarctic Peninsula since 1945: observations and possible causes. *Ann Glaciol* 27: 571-575.

- KONZ M. 2011. Transient Snowline. In: Singh VP, Singh P & Haritashya UK (Eds), *Encyclopedia of Snow, Ice and Glaciers*. Dordrecht: Springer, p. 1203-1203.
- LEWIS AJ & HENDERSON FM. 1998. Radar fundamentals: The Geoscience Perspective. In: HENDERSON FM & LEWIS AJ (Orgs), *Principles & Applications of Imaging Radar: manual of remote sensing*. New York: John Willey, p. 131-181.
- LI D, SHANGGUAN D & ANJUM MN. 2020. Glacial Lake inventory derived from Landsat 8 OLI in 2016-2018 in China-Pakistan economic corridor ISPRS Int J Geo-Inf 9: 294.
- LI Y, DING Y, SHANGGUAN D & WANG R. 2019. Regional differences in global glacier retreat from 1980 to 2015. *Adv Clim Chang Res* 10: 203-213.
- LLANILLO PJ, AIKEN CM, CORDERO RR, DAMIANI A, SEPÚLVEDA E & FERNADÉZ-GÓMEZ B. 2019. Oceanographic variability induced by tides, the intraseasonal cycle and warm subsurface water intrusions in Maxwell Bay, King George Island (West-Antarctica). *Sci Rep* 9: 18571.
- MÄKYNEN MP, MANNINEN AT, SIMILA MH, KARVONEN JA & HALLIKAINEN MT. 2002. Incidence angle dependence of the statistical properties of C-band HH-polarization backscattering signatures of the Baltic Sea ice. *IEEE Trans Geosci Remote Sens* 40: 2593-2605.
- MARSHALL GJ, ORR A, VAN LIPZIG NP & KING JC. 2006. The impact of a changing Southern Hemisphere Annular Mode on Antarctic Peninsula summer temperatures. *J Clim* 19(20): 5388-5404.
- MCFEETERS SK. 1996. The use of the Normalized Difference Water Index (NDWI) in the delineation of open water features. *Int J of Remote Sens* 17: 425-1432.
- MEREDITH MP & KING JC. 2005. Rapid climate change in the ocean west of the Antarctic Peninsula during the second half of the 20th century. *Geophys* 32: L19604.
- MOFFAT C & MEREDITH M. 2018. Shelf-ocean exchange and hydrography west of the Antarctic Peninsula: a review. *Phil Trans R Soc A* 376: 2122.
- MORRIS J, POOLE A & KLEIN A. 2006. Retreat of tropical glaciers in Colombia and Venezuela from 1984 to 2004 as measured from ASTER and Landsat Images. In: 63^o Eastern Snow Conference. Newark, Delaware, EUA. 181-191.
- NESJE A. 1992. Topographical effects on the equilibrium-line altitude on glaciers. *GeoJournal* 27: 383-397.
- NESJE A & DAHL SO. 2000. *Glaciers and Environmental Change. Key issues in environmental Change*. Hodder Education, 203 p.
- NIE Y, LIU Q & LIU S. 2013. Glacial lake expansion in the central Himalayas by Landsat images, 1990-2010. *PLOS ONE* 9: E92654.
- OLIVA M, NAVARRO F, HRBÁČEK F, HENÁNDEZ A, NÝVLT D, PEREIRA P, RUIZ-FERNÁNDEZ J & TRIGO R. 2017. Recent regional climate cooling on the Antarctic Peninsula and associated impacts on the cryosphere. *Sci Total Environ* 580: 210-223.
- OLIVEIRA MAG, ROSA KK, PETSCH C & SIMÕES JC. 2019. Variação de área das geleiras do campo de gelo Kraków, ilha Rei George, Antártica, no período entre 1956 e 2017. *Revista Caminhos de Geografia* 20: 55-71.
- OLIVEIRA MAG, ROSA KK, PETSCH C, VIEIRA R, CASANOVA F & SIMÕES JC. 2021. Mudanças recentes (1988-2018) em áreas livres de gelo nas ilhas Nelson e Rei George, Antártica Marítima. *Rev Bras Geomorf* 22: 562-577.
- OSMANOĞLU B, BRAUN M & NAVARRO FJ. 2013. Surface velocity and ice discharge of the ice cap on King George Island, Antarctica. *Ann Glaciol* 54: 111-119.
- PAN B, CAO B, WANG J, ZHANG G, ZHANG C, HY Z & HUANG B. 2012. Glacier variations in response to climate change from 1972 to 2007 in the western Lenglongling mountains, northeastern Tibetan Plateau. *J Glaciol* 58: 879-888.
- PATERSON WSB. 1994. *Physics of Glaciers*. Elsevier Science & Technology. Oxford. 3^a ed. 480 p.
- PAUL F ET AL. 2015. The glaciers climate change initiative: Methods for creating glacier area, elevation change and velocity products. *Remote Sens Environ* 162: 408-426.
- PERONDI C, ROSA KK & VIEIRA R. 2019. Caracterização geomorfológica das áreas livres de gelo na margem leste do campo de gelo Warszawa, Ilha Rei George, Antártica marítima. *Rev Bras Geomorf* 20: 411-426.
- PERONDI C, ROSA KK, PETSCH C, IDALINO FD, OLIVEIRA MAG, LORENZ JL, VIEIRA R & SIMÕES JC. 2020. Recentes alterações nas geleiras e nos sistemas paraglaciais, Antártica Marítima. *REGNE* 6: 292-301.
- PETSCH C, SOTILLE ME, COSTA RM, ROSA KK & SIMÕES JC. 2019. Cambios climáticos y aumento de la vegetación en la Península Fildes, Antártica. *Invest Geogr* 57: 18-31.
- PETSCH C, ROSA KK, VIEIRA R, BRAUN MH, COSTA RM & SIMÕES JC. 2020. Los efectos de los cambios climáticos en los sistemas glaciales, proglaciales y periglaciales del glaciar Collins, isla Rey Jorge, Antártica, del final de la Pequeña Edad del Hielo al siglo XXI. *Invest Geogr* 103.
- POELKING EL, ANDRADE AM, VIEIRA GB, SCHAEFER CE & FERNANDES FILHO EI. 2014. Variações da frente da geleira Polar Club, Península Potter (Ilha Rei George, Antártica

- Marítima) entre 1986 e 2011. *Rev Bras Meteorol* 29: 379-388.
- PUDEŁKO R, ANGIEL P, POTOCKI M, JĘDREJEK A & KOZAK M. 2018. Fluctuation of glacial retreat rates in the eastern part of Warszawa Icefield, King George Island, Antarctica, 1979-2018. *Remote Sens* 10: 892.
- RACOVITEANU AE, ARNAUD Y, WILLIAMS M & ORDOÑEZ J. 2008. Decadal changes in glacier parameters in the Cordillera Blanca, Peru, derived from remote sensing. *J Glaciol* 54: 499-510.
- RAU F, BRAUN MH, FRIEDRICH M, WEBER F & GOßMANN H. 2000. Radar glacier zones and their boundaries as indicators of glacier mass balance and climatic variability. *Proceedings of EARSeL-SIG-Workshop Land Ice and Snow, Dresden/FRG* 1: 317-327.
- REEH N, THOMSEN HH, HIGGINS AK & WEIDICK A. 2001. Sea ice and the stability of north and northeast Greenland floating glaciers, *Ann Glaciol* 33: 474-480.
- REKOWSKY IC, BREMER UF & VEETIL BK. 2019. Variações de área das geleiras da Colômbia e da Venezuela entre 1985 e 2015, com dados de sensores remoto. *Rev Geociências (UNESP)* 37: 569-581.
- RIGNOT E, GOGINENI S, JOUGHIN I & KRABILL W. 2001. Contribution to the glaciology of northern Greenland from satellite radar interferometry. *J. Geophys. Res Atmos* 106: 34007-34019.
- RIGNOT E & STEFFEN K. 2008. Channelized bottom melting and stability of floating ice shelves. *Geophys Res Lett* 35: 2-6.
- ROE G, BAKER M & HERLA F. 2017. Centennial glacier retreat as categorical evidence of regional climate change. *Nat Geosci* 10: 95-99.
- ROSA KK, PERONDI C, VEETIL BK, AUGER JD & SIMÕES JC. 2020. Contrasting responses of land-terminating glaciers to recent climate variations in King George Island, Antarctica. *Antarct Sci* 32: 398-407.
- ROSA KK, SARTORI RB, MENDES JR CW & SIMÕES JC. 2015a. Análise das mudanças ambientais da geleira Viéville, Baía do Almirantado, Ilha Rei George, Antártica. *Pesquisas em Geociências* 42: 61-71.
- ROSA KK, SOUZA JUNIOR E, VIEIRA R & SIMÕES JC. 2014. The landforms and pattern of deglaciation of the Dragon glacier, King George Island, South Shetlands, Antarctica. *Revista de Geografia* 30: 6-16.
- ROSA KK, VIEIRA R, FERNANDEZ G, MENDES JR CW, VELHO LF & SIMÕES JC. 2015b. Recent changes in the Wanda Glacier, King George Island, Antarctica. *Pesquisas em Geociências* 42: 187-196.
- ROSA KK, VIEIRA R, SIMÕES JC & FERRANDO FJ. 2009. Feições sedimentológicas e geomorfológicas do ambiente de deglaciação das geleiras Wanda e Ecology, ilha Rei George - Antártica. *Pesquisas em Geociências* 37: 315- 326.
- ROSA KK, OLIVEIRA MAG, PETSCH C, AUGER JD, VIEIRA R & SIMÕES JC. 2021. Expansion of glacial Lakes on Nelson and King George Islands, Maritime Antarctica, from 1986 to 2020. *Geocarto Int* 1-9.
- RÜCKAMP M, BLINDOW N, SUCKRO SK, BRAUN MH & HUMBERT A. 2012. Measured ice surface velocities on the King George Island ice cap with DGPS. PANGEA. Available in: <<https://doi.org/10.3189/172756410791392817>>. Access in: 09 dec 2021.
- RÜCKAMP M, BRAUN M, SUCKRO S & BLINDOW N. 2011. Observed glacial changes on the King George Island ice cap, Antarctica, in the last decade. *Global Planet Change* 79: 99-109.
- SANCHES AM, VELHO LF & SIMOES, JC. 2015. Fluctuaciones en la extensión de los glaciares del nevado Cololo (14°50' L.S. - 69°10' L.W.) a partir de datos de TM/LANDSAT-5. *Acta geológica lilloana* 27: 121-129.
- SHAHATEET K, SEEHAUS T, NAVARRO F, SOMMER C & BRAUN M. 2021. Geodetic Mass Balance of the South Shetland Islands Ice Caps, Antarctica, from Differencing TanDEM-X DEMs. *Remote Sens* 13: 3408.
- SHIMABUKURO YE & SMITH JA. 1991. The least-squares mixing models to generate fraction images derived from remote sensing multispectral data. *IEEE Trans Geosci Remote Sens* 29: 16-20.
- SILVA AB, ARIGONY-NETO J, BRAUN M, ESPINOZA JM, COSTI J & JAÑA R. 2020. Spatial and temporal analysis of changes in the glaciers of the Antarctic Peninsula. *Global Planet Change* 184: 103079.
- SILVERIO W & JAQUET JM. 2012. Multi-temporal and multi-source cartography of the glacial cover of Nevado Coropuna (Arequipa, Peru) between 1955 and 2003. *Int J Remote Sens* 33: 5876-5888.
- SIMÕES JC, BREMER UF, AQUINO FE & FERRON FA. 1999. Morphology and variations of glacial drainage basins in the King George Island ice field, Antarctica. *Ann Glaciol* 29: 220-224.
- SIMÕES CL, ROSA KK, CZAPELA FF, VIEIRA R & SIMÕES JC. 2015. Collins Glacier retreat process and regional climatic variations, King George Island, Antarctica. *Geogr Rev* 105: 462-471.

- SIMÕES CL, ROSA KK, SIMÕES JC, VIEIRA R, COSTA RM & SILVA AB. 2020. Recent changes in two outlet glaciers in the Antarctic Peninsula using multi-temporal Landsat and Sentinel-1 data. *Geoc Int* 35: 1233-1244.
- SMITH L, FORSTER R, ISACKS B & HALL D. 1997. Seasonal climatic forcing of alpine glaciers revealed with orbital synthetic aperture radar. *J Glaciol* 43: 480 - 488.
- SOBOTA I, KEJNA M & ARAŽNY A. 2015. Short-term mass changes and retreat of the Ecology and Sphinx glacier system, King George Island, Antarctic Peninsula. *Antarct Sci* 27: 500-510.
- SOTILLE M, BREMER UF & SIMÕES JC. 2016. Avanço e retração de área glacial no extremo norte da península Trinity, Antártica, entre 1988 e 2015. *Revista do Departamento de Geografia (USP)* 31: 72-81.
- STOKES CR, SANDERSON JE, MILES BWJ, JAMIESON SSR & LEESON AA. 2019. Widespread distribution of supraglacial lakes around the margin of the East Antarctic Ice Sheet. *Sci Rep* 9: 13823.
- SZİŁO J & BIALIK R. 2018. Recession and ice surface elevation changes of Baranowski Glacier and its impact on proglacial relief (King George Island, West Antarctica). *Geosci* 8: 355.
- THOMAS R, FREDERICK E, KRABILL W, MANIZADE S & MARTIN C. 2009. Recent changes on Greenland outlet glaciers. *J. Glaciol* 55: 147-162.
- TURNER J, COLWELL SR, MARSHALL GJ, LACHLAN-COPE TA, CARLETON AM, JONES PD, LAGUN V, REID PA & IAGOVKINA S. 2005a. Antarctic climate change during the last 50 years. *Int J Climatol* 25: 279-294.
- TURNER J, LACHLAN-COPE T, COLWELL S & MARSHALL GJ. 2005b. A positive trend in western Antarctic Peninsula precipitation over the last 50 years reflecting regional and Antarctic-wide atmospheric circulation changes. *Ann Glaciol* 41: 85-91.
- TURNER J, LU H, KING J, MARSHALL G, PHILLIPS T, BANNISTER D & COLWELL S. 2021. Extreme temperatures in the Antarctic. *J Clim* 34: 2653-2668.
- TURNER J, LU H, KING J, PHILLIPS T, HOSKING JS, BRACEGIRDLE TJ, MARSHALL G, MULVANEY R & DEB P. 2016. Absence of 21st century warming on Antarctic Peninsula consistent with natural variability. *Nature* 535: 411-415.
- VAUGHAN DG ET AL. 2003. Recent Rapid Regional Climate Warming on the Antarctic Peninsula. *Clim Change* 60: 243-274.
- VELHO LF, ARIGONY NETO J & SIMÕES JC. 2011. Utilização do filtro Lee na redução do speckle em imagens SAR usadas na determinação da velocidade de geleiras. *RBC* 253-265.
- ZHANG G, YAO T, XIE H, WANG W & YANG W. 2015. An inventory of glacial lakes in the Third Pole region and their changes in response to global warming. *Global Planet Change* 131: 148-157.
- ZHOU C & ZHENG L. 2017. Mapping Radar Glacier Zones and Dry Snow line in the Antarctic Peninsula Using Sentinel-1 Images. *Remote Sensing* 9: 1171.
- ZHOU C, LIU Y & ZHENG L. 2021. Satellite-derived dry-snow line as an indicator of the local climate on the Antarctic Peninsula. *J Glaciol* 1-11.

How to cite

LORENZ JL, ROSA KK, PETSCH C, PERONDI C, IDALINO FD, AUGER JD, VIEIRA R & SIMÕES JC. 2023. Short-term glacier area changes, glacier geometry dependence, and regional climatic variations forcing, King George Island, Antarctica. *An Acad Bras Cienc* 95: e20211627. DOI 10.1590/0001-3765202320211627.

*Manuscript received on December 29, 2021;
accepted for publication on September 4, 2022*

JÚLIA L. LORENZ¹

<https://orcid.org/0000-0003-1695-1807>

KÁTIA K. DA ROSA¹

<https://orcid.org/0000-0003-0977-9658>

CARINA PETSCH^{1,2}

<https://orcid.org/0000-0002-1079-0080>

CLEIVA PERONDI¹

<https://orcid.org/0000-0003-2202-2721>

FILIPE D. IDALINO¹

<https://orcid.org/0000-0001-5587-5208>

JEFFREY DANIEL AUGER¹

<https://orcid.org/0000-0002-2304-2292>

ROSEMARY VIEIRA³

<https://orcid.org/0000-0003-0312-2890>

JEFFERSON C. SIMÕES¹

<https://orcid.org/0000-0001-5555-3401>

¹Universidade Federal do Rio Grande do Sul, Centro Polar e Climático, Avenida Bento Gonçalves, 9500, Agronomia, 91501-970 Porto Alegre, RS, Brasil.

²Universidade Federal de Santa Maria, Programa de Pós-graduação em Geografia, Avenida Roraima 1000, 97105-900 Santa Maria, RS, Brazil

³Universidade Federal Fluminense, Laboratório de Processos Sedimentares e Ambientais, Departamento de Geografia, Campus da Praia Vermelha, Avenida General Milton Tavares de Souza, s/n, 24210-346 Niterói, RJ, Brazil

Correspondence to: **Júlia Lopes Lorenz**

E-mail: jlopeslorenz@gmail.com

Author contributions

Julia Lopes Lorenz: conceptualization, methodology, formal analysis, investigation, writing, reviewing. Kátia Kellem da Rosa: conceptualization, methodology, formal analysis, investigation, writing, reviewing. Carina Petsch: methodology, formal analysis, investigation, writing, reviewing. Felipe Daros Idalino and Cleiva Perondi: conceptualization, methodology, investigation. Jeffrey: methodology, investigation, formal analysis, writing, reviewing, translating. Rosemary Vieira: formal analysis, writing, reviewing. Jefferson Cardia Simões: project administration, reviewing.

